Supplementary material

Optically Detected Magnetic Resonance of Silicon Vacancies in 4H-SiC at Elevated Temperatures toward Magnetic Sensing under Harsh Environments

Shu Motoki（元木 秀）[1,2], Shin-ichiro Sato（佐藤 真一郎）[2], Seiichi Saiki（佐伯 誠一）[2], Yuta Masuyama（増山 雄太）[2], Yuichi Yamazaki（山﨑 雄一）[2], Takeshi Ohshima（大島 武）[2], Koichi Murata（村田 晃一）[3], Hidekazu Tsuchida（土田 秀一）[3], Yasuto Hijikata（土方 泰斗）[1]

[1]Graduate School of Science and Engineering, Saitama University, Saitama 338-8570, Japan
[2]National Institutes for Quantum Science and Technology, Takasaki, Gunma 370-1292, Japan
[3]Central Research Institute of Electric Power Industry, Yokosuka, Kanagawa 240-0196, Japan

Corresponding author: sato.shinichiro2@qst.go.jp (S.-I. Sato)

S1. Characterization of V_{Si}^{-}(k) concentration

In ESR measurements, the signal intensity saturates at high microwave (MW) power because the relaxation process does not recover to the equilibrium state, resulting in an underestimation of the spin number in the sample. We first analyzed the MW power dependence of the integrated ESR intensity to accurately characterize the T_{V2a} center (V_{Si} defect) concentration. Figure S1 (a) and (b) show the ESR spectra of T_{V2a} center at different MW powers (electron fluence: 5.0×10^{18} cm^{-2}) and the MW power dependence of the integrated ESR intensity. The signal intensity showed a saturation trend at the power above 1 μW. Therefore, the MW power at 0.4 μW was used for all the samples to quantify the V_{Si}^{-}(k) concentration.

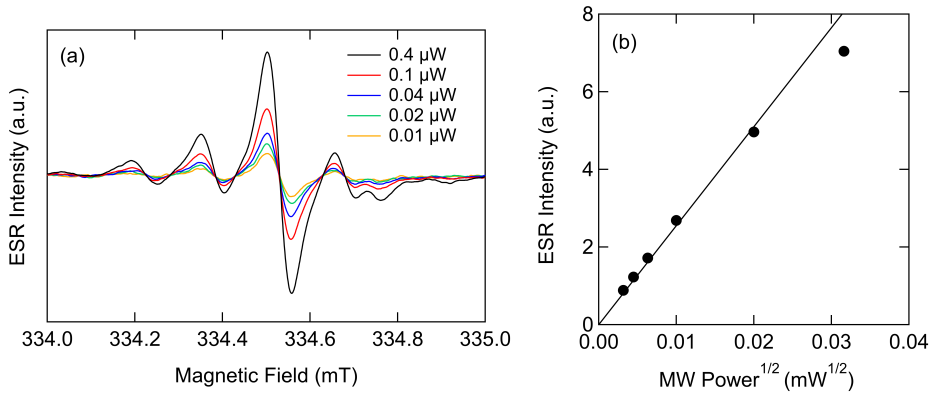

Fig. S1. (a) ESR spectra of T_{V2a} centers with different MW powers (0.01 – 0.4 μW) for B || c at room temperature [electron fluence: 5.0×10^{18} cm^{-2}, modulation field: 0.05 mT, modulation frequency: 100 kHz]. (b) The integrated T_{V2a} signal intensity as a function of the square root of the MW power.

Figure S2 (a) shows DLTS spectra of n-type 4H-SiC Schottky diodes with a doping concentration of 2×10^{17} cm^{-3}. Two types of samples with different initial nitrogen doping concentrations were measured to characterize the S_1 and $Z_{1/2}$ centers (open symbols: 4×10^{15} cm^{-3}, closed symbols: 2×10^{17} cm^{-3}). A peak related to the S_1 center, which was the transition of V_{Si} defects from −3 to −2 charge states (=V_{Si} (−2|−3)), was observed at 200 K, and also, a peak related to the $Z_{1/2}$ defects, which was the transition of the h-site (Z_1) and k-site (Z_2) carbon vacancies (=V_C) from −1 to 0 charge states (=V_C (−1|0)), was observed at 300 K [1-5]. Fig. S2 (b) shows the change in $Z_{1/2}$ concentration as a function of electron fluence, which was derived from the peak intensities. The $Z_{1/2}$ concentration was slightly reduced after annealing at 600 ºC.

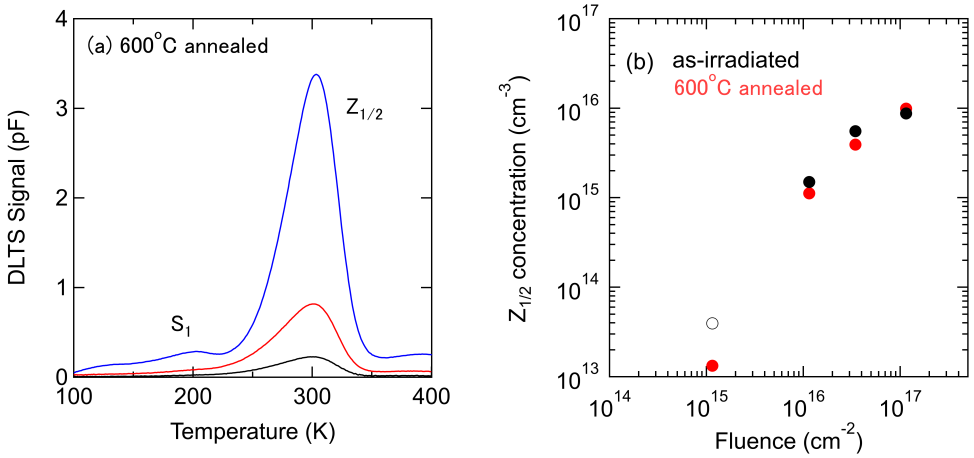

Fig. S2. (a) DLTS spectra of n-type 4H-SiC Schottky diodes (doping concentration: 2×10^{17} cm^{-3}) after electron irradiation at the fluence of 1.1×10^{16} cm^{-2} (black), 3.4×10^{16} cm^{-2} (red), and 1.1×10^{17} cm^{-2} (blue). (b) The $Z_{1/2}$ concentrations as a function of electron irradiation fluence from 1.1×10^{15} to 1.1×10^{17} cm^{-2}. Black and red symbols are the experimental data for as-irradiated and 600 °C annealed samples, respectively. Open and closed symbols denote the data obtained from the diodes with doping concentrations of 4×10^{15} cm^{-3} and 2×10^{17} cm^{-3}, respectively.

S2. Distance and Depth Dependence of ODMR Spectra

Since ODMR contrast is highly dependent on RF power applied to V_{Si}^{-}(k), we first measured the distance and depth dependence of the ODMR signal to obtain repeatability. Figure S3 (a) shows a confocal XY mapping (X×Y=100×100 μm^2) of the sample surface. The PL emission was clearly observed throughout the entire region except for the Cu electrode. The depth dependence of the ODMR contrast from the sample surface is shown in Fig. S3 (b). The ODMR contrast decreased with increasing the distance from the Cu electrode. On the other hand, the ODMR contrast was almost independent of the depth from the surface as shown in Fig.S3 (c). Based on these results, we set (distance, depth) = (20 μm, 20 μm) for ODMR measurements for repeatability.

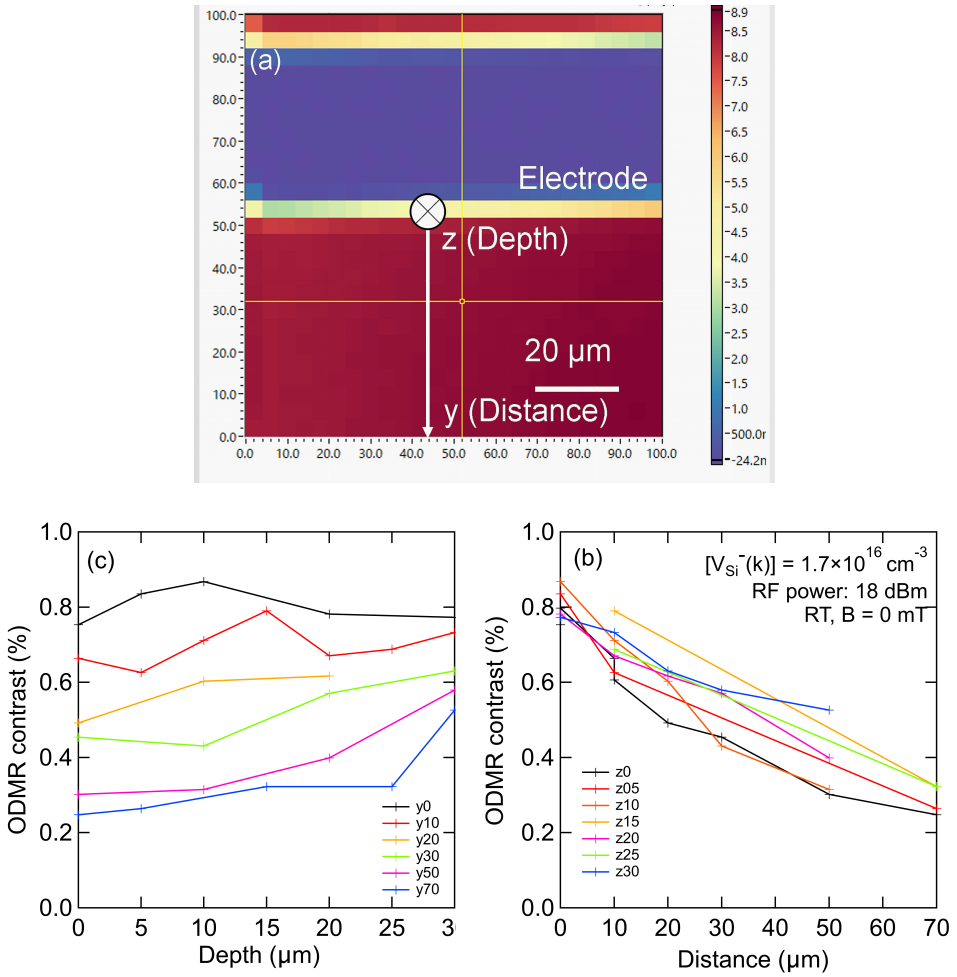

Fig. S3. (a) A confocal microscopy image of V_{Si}^{-}(k) defects on the surface of a 4H-SiC sample with an excitation laser power of 45 mW (100 × 100 μm^2). (b) ODMR contrast as a function of the distance from the electrode edge on the sample. (c) ODMR contrast as a function of depth from the surface of the 4H-SiC sample. The ODMR measurements were conducted at room temperature.

S3. Sample Variations on Temperature Dependence of PL Intensities

Low-temperature PL measurements were performed to confirm the formation of V_{Si}^- defects. Figure S4 shows the PL spectra after electron irradiation at 3.4×10^{18} cm^{-2} at low (80 K) and room (300 K) temperatures. At low temperatures, two characteristic peaks appeared at 859.8 nm and 916.3 nm which are attributed to the zero phonon lines (ZPLs) of two non-equivalent lattice sites; h-site (V1 center) and k-site (V2 center) [6-8]. Figure S4 (b)–(d) shows PL spectra at temperatures from 300 K to 591 K for different samples. No significant change in PL spectra due to annealing at 600 ºC was found. Also, no significant change in PL spectra due to irradiation fluence was found. The change in relative PL intensity of V_{Si}^- defects as a function of temperature for different samples is shown in Fig. S4 (e). The PL intensity was normalized by the value at 300 K. Unlike the other samples, the PL intensity of the 1.3×10^{19} cm^{-2} irradiated sample slightly decreased at high temperatures (closed circles in (e)). This is presumably because the sample temperatures during irradiation were slightly different for each sample and other defects that could cause quenching of V_{Si}^- defects at high temperatures were formed on a certain condition. Further investigation is necessary to clarify this.

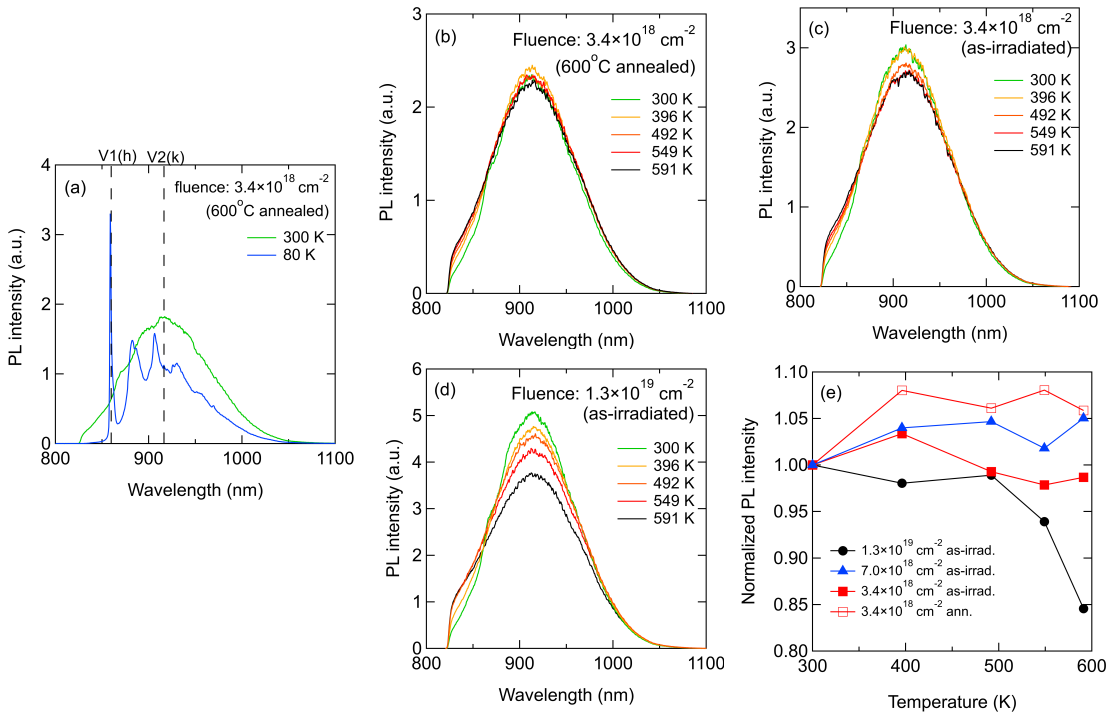

Fig. S4. (a) PL spectra of V_{Si}^- in 4H-SiC at low (80 K) and room (300 K) temperatures. (b)–(d) Sample variations of PL spectra with different temperatures. The irradiation fluence is (b) 3.4×10^{18} cm^{-2} with 600 ºC annealed, (c) 3.4×10^{18} cm^{-2} as-irradiated, (d) 1.3×10^{19} cm^{-2} as-irradiated and (e) normalized PL intensity as a function of temperature. The PL intensity was normalized by the value at 300 K.

S4. ODMR Spectra of the Maximum Fluence in This Study

Figure S5 shows the ODMR spectra at room temperature for the V_{Si}^{-}(k) concentration of 6.0×10^{16} cm^{-3}, which was the maximum electron irradiation fluence (1.3×10^{19} cm^{-2}) in this study. The resonance peak at 70.3 MHz was observed under zero magnetic field and was split into two by the Zeeman splitting (resonance frequency of ν1=40.5 MHz and ν2=99.2 MHz) when 1 mT external magnetic field was applied.

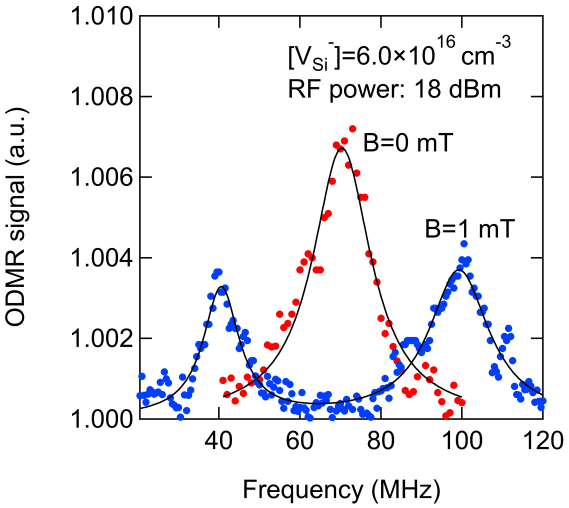

Fig. S5. The ODMR spectra at room temperature at V_{Si}^{-}(k) concentration of 6.0×10^{16} cm^{-3} with external magnetic fields for B || c (1 mT) and without external magnetic field.

S5. Radiation Resistance of V_{Si}^-

To demonstrate the radiation resistance of V_{Si}^- spin properties, we performed γ-ray irradiation on a V_{Si}^- formed HPSI 4H-SiC and investigated the PL and ODMR properties. Fig. S6 (a) shows the PL spectra of V_{Si}^- defects before and after γ-ray irradiation at 19 kGy (H_2O) and 119 kGy (H_2O). The samples were irradiated with 2 MeV electrons at the fluence of 2.5×10^{18} cm^{-2} before γ-ray irradiation. Note that 10 kGy is roughly equivalent to an absorption dose for 10 years in the geostationary orbit (GEO) in space. As a result, no significant change in PL spectrum and intensity was observed after γ-ray irradiation, indicating that V_{Si}^- defects show stable luminescence under radiation environments. The ODMR spectra under zero magnetic field and 1 mT for B || c after γ-ray irradiations are shown in Fig. S6 (b)–(d). The ODMR contrast (%), resonance frequency (MHz), and FWHM (MHz) extracted by fitting the Lorentz function are listed in Table S1. In these measurements, the RF radiation was directed to a thin copper wire terminated with a 50 ohm impedance. The resonance peak around 70 MHz due to the zero-field splitting of the V_{Si}^-(k) ground states and its Zeeman splitting due to the external magnetic field were observed in all the samples. No significant change in the ODMR spectra was observed at any γ-ray dose. These results strongly suggest that V_{Si}^- magnetic sensors can be used in a radiation environment without any deterioration.

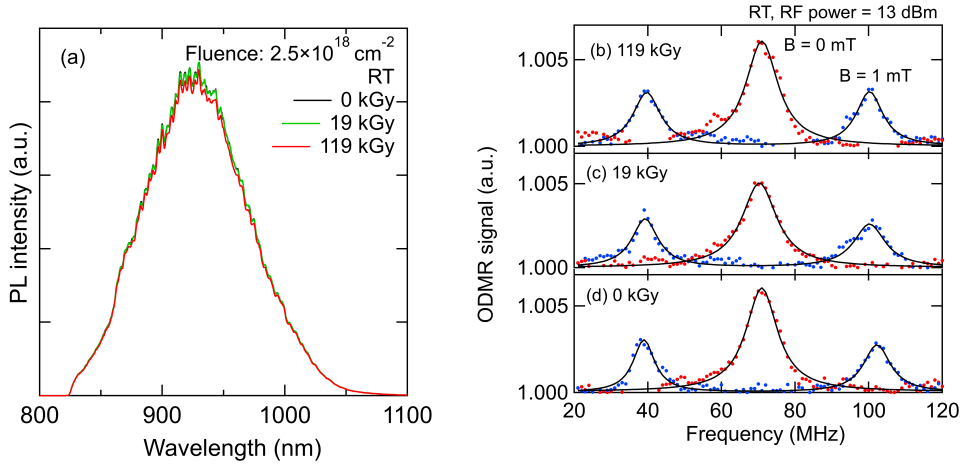

Fig. S6. (a) PL spectra at room temperature before and after γ-ray irradiation. (b), (c) and (d) show the ODMR spectra at room temperature after γ-ray irradiations at 119 kGy(H_2O), 19 kGy(H_2O), and 0 kGy(H_2O), respectively.

Table S1. Parameters extracted from the Lorentzian fit.

0 mT				1 mT ν1/ν2			
γ (kGy)	Contrast (%)	Freq. (MHz)	FWHM (MHz)	γ (kGy)	Contrast (%)	Freq. (MHz)	FWHM (MHz)
0	0.60	70.9	10.4	0	0.29/0.26	39.2/100.2	8.6/10.3
19	0.50	70.3	11.4	19	0.31/0.32	39.7/100.2	9.0/8.8
119	0.61	70.1	10.7	119	0.30/0.26	38.9/102.2	7.0/8.1

S6. Calculation of Displacement per Atom (dpa)

The displacement per atom, C_d is defined by the following equation [9]:

$$C_\mathrm{d} = \frac{N_\mathrm{d}}{N} = t\varphi \int_{E_\mathrm{d}}^{E_\mathrm{pmax}} \nu(E_\mathrm{p}) \frac{d\sigma_\mathrm{p}}{dE_p}\, dE_p \tag{S1},$$

where N, N_d, t, φ, E_d, E_p, E_pmax, and σ_p are the atomic density of the target material, the number of displacements per volume, the electron irradiation time, the electron beam flux, the displacement energy, the energy of primary knock-on atom (PKA), the maximum PKA energy, and the total cross section for atomic displacement. In the case of relativistic electron irradiation, σ_p is represented as follows:

$$d\sigma_\mathrm{p}(E, E_\mathrm{p}) = \frac{\pi b'^2}{4}\left[1 - \beta^2 \frac{E_\mathrm{p}}{E_\mathrm{pmax}} + \pi\alpha\beta\left\{\left(\frac{E_\mathrm{p}}{E_\mathrm{pmax}}\right)^{1/2} - \frac{E_\mathrm{p}}{E_\mathrm{pmax}}\right\}\right] \times \frac{E_\mathrm{pmax}}{{E_\mathrm{p}}^2} dE_\mathrm{p} \tag{S2},$$

$$\alpha = \frac{Z_2 e^2}{\hbar c} = \frac{Z_2}{137.04} \tag{S3},$$

$$\beta = \sqrt{1 - \left(\frac{m_0 c^2}{m_0 c^2 + E}\right)^2} \tag{S4},$$

$$b' = b\sqrt{1 - \beta^2} \tag{S5},$$

$$b \cong \frac{2Z_2 e^2}{m_0 c^2 \beta^2} \tag{S6},$$

where b is the distance of the closest approach and b' is the relativistically corrected b. Z_2, e, $\hbar$, c, E, and m_0 are the charge number of the target nucleus, the elementary charge, the Plank constant, the speed of light, and the acceleration energy of electrons.

The displacement damage function, $\nu(E_\mathrm{p})$ in Eq. (S1) represents how many displacements occur from one PKA. In the Kinchin-Peace model, which is one of the most widely used and the simplest models, $\nu(E_\mathrm{p})$ is represented as follows:

$$\nu(E_\mathrm{p}) = \begin{cases} 0 & (0 \le E_\mathrm{p} \le E_\mathrm{d}) \\ 1 & (E_\mathrm{d} \le E_\mathrm{p} \le 2E_\mathrm{d}) \\ E_\mathrm{p}/2E_\mathrm{d} & (2E_\mathrm{d} \le E_\mathrm{p} \le E_\mathrm{pmax}) \end{cases} \tag{S7}.$$

E_pmax of PKA formed by relativistic electrons is not so high that the energy loss of PKA through ionizations and electronic excitations is almost negligible. For instance, when carbon (C) is irradiated with 2 MeV electrons, E_pmax is calculated to be:

$$E_\mathrm{pmax} = 2E\left(\frac{E + 2m_0 c^2}{M_2 c^2}\right) = 1{,}081\ (\mathrm{eV}) \gg 2E_\mathrm{d} \tag{S8},$$

where M_2 is the atomic mass of the target material. Thus, the PKA energy is mainly lost by elastic collisions. Eq. (S1) can be rewritten using Eq. (S7):

$$C_{\mathrm{d}} = t\varphi\left\{\int_{E_{\mathrm{d}}}^{2E_{\mathrm{d}}} \frac{d\sigma_{\mathrm{p}}}{dE_p}\, dE_p + \int_{2E_{\mathrm{d}}}^{E_{\mathrm{pmax}}} \frac{E_{\mathrm{p}}}{2E_{\mathrm{d}}}\, \frac{d\sigma_{\mathrm{p}}}{dE_p}\, dE_p\right\} \quad \text{(S9)},$$

and this can be solved analytically:

$$C_{\mathrm{d}} = \frac{t\varphi\pi b'^2}{4}\left\{\frac{x}{2}\left(\ln\frac{x}{2}+1\right) - \beta^2\left(\frac{x}{2}+\ln 2-1\right) + \pi\alpha\beta\left(\frac{x}{2}-2x^{\frac{1}{2}}+1-\ln 2\right)\right\} \quad \text{(S10)},$$

$$x = \frac{E_{\mathrm{pmax}}}{E_{\mathrm{d}}} \quad \text{(S11)}.$$

Since the composition ratio of SiC is Si:C =1:1, the value of dpa, C_{dSiC} can be simply calculated as the sum of C_{dSi} and C_{dC} (Bragg's additive law):

$$C_{\mathrm{dSiC}} = \frac{1}{2}(C_{\mathrm{dSi}}+C_{\mathrm{dC}}) \quad \text{(S12)}.$$

When E = 2 MeV and $t\varphi$ = 1.3×10^{19} cm^{-2} (electron fluence), C_{dSiC} is calculated to be 5.4×10^{-4} dpa from the Eq. (S12) with E_{d} = 25 eV for Si and 21 eV for C [10].

References

[1] M. E. Bathen, A. Galeckas, J. Müting, H. M. Ayedh, U. Grossner, J. Coutinho, Y. K. Frodason, and L. Vines, npj Quantum Inf. **5**. 111 (2019).

[2] I. Capan, T. Brodar, Z. Pastuovic, R. Siegele, T. Ohshima, S.-I. Sato, T. Makino, L. Snoj, V. Radulovic, J. Coutinho, V. J. B. Torres, and K. Demmouche, J. Appl. Phys. **123**, 161597 (2018).

[3] I. Capan, T. Brodar, J. Coutinho, T. Ohshima, V. P. Markevich, and A. R. Peaker, J. Appl. Phys. **124**, 245701 (2018).

[4] N. T. Son, X. T. Trinh, L. S. Lovlie, B. G. Svensson, K. Kawahara, J. Suda, T. Kimoto, T. Umeda, J. Isoya, T. Makino, T. Ohshima, and E. Janzen, Phys. Rev. Lett. **109**, 187603 (2012).

[5] I. Capan, Y. Yamazaki, Y. Oki, T. Brodar, T. Makino, and T. Ohshima, Crystals, **9**, 328 (2019).

[6] E. Sorman, N. T. Son, W. M. Chen, O. Kordina, C. Hallin, and E. Jnzen, Phys. Rev. B **61**, 2613–2620 (2000).

[7] F. Fuchs, B. Stender, M. Trupke, D. Simin, J. Pflaum, V. Dyakonov, and G. V. Astakhov, Nat. Comm. **6**, 7578 (2015).

[8] S.-I. Sato, T. Narahara, Y. Abe, Y. Hijikata, T. Umeda, and T. Ohshima, J. Appl. Phys. **126**, 083105 (2019).

[9] S. Ishino [Nuclear Engineering Series 8: Radiation Damage] *Genshiryoku kougaku series 8: Shousha Sonshou* (in Japanese), (the University of Tokyo Press, 1979) Chapter 3, pp.23–49.

[10] J. W. Steeds, G. A. Evans, L. R. Danks, S. Furkert, W. Voegeli, M. M. Ismail, and F. Carosella, Diamond Relat. Mater. **11(12)**, 1923–1945 (2002).